

Evolution of Power Spectrum in the Little Bangs

Golam Sarwar^{a,b}, Sushant K. Singh^{a,b}, Jan-e Alam^{a,b}.

^a Variable Energy Cyclotron Centre, 1/AF, Bidhan Nagar, Kolkata - 700064, INDIA, ^bHomi Bhabha National Institute, Mumbai, India.

The power spectrum of fluctuations in the momentum distributions of particles have been estimated with optical Glauber and Monte-Carlo Glauber initial conditions for relativistic heavy ion collisions. The evaluation procedure adopted in this work is analogous to the one used in the calculation of power spectrum in Cosmic Microwave Background Radiation (CMBR). The power spectrum due to perturbations in the phase space distribution of the particles which drive the system away from equilibrium have also been evaluated. The phase space perturbation has been evolved through the Boltzmann transport equation in an expanding quark gluon plasma (QGP) background. The expansion of the QGP has been treated within the ambit of relativistic hydrodynamics. We observe that the non-equilibrium effects introduced as perturbations in the phase space distributions can be traced from the enhancement of the power spectrum as well as through its variation with temperature which is distinctly different from the case of vanishing perturbation. A relation between the power spectrum with the flow harmonics has been derived which can be used to estimate various flow harmonics and its fluctuations and dependence on kinematic variables.

PACS numbers:

I. INTRODUCTION

The renormalization group approach in Quantum Chromodynamics (QCD) predicts that at high density and temperature (T) hadronic matter undergoes a phase transition to quark matter [1] due to asymptotic freedom [2, 3] and Debye screening of colour charges. Calculations based on lattice QCD has predicted that the transition from hadronic to quark matter takes place in the temperature domain, $145 \leq T(\text{MeV}) \leq 163$ [4–6] at negligible baryon density. At Relativistic Heavy Ion Collider (RHIC) and Large Hadron Collider (LHC) heavy nuclei are made to collide to create quark matter or quark gluon plasma (QGP) - a state of matter that prevailed in the micro-second old universe according to the cosmological Big Bang (BB) model. In this regard the production of QGP in nuclear collisions at relativistic energies is dubbed as Little Bangs (LB). One of the compulsion to study the QCD phase transition in Heavy Ion Collisions at Relativistic Energies (HICRE) is to understand the non-abelian gauge theory in medium and to understand the dynamics of similar transition in the early universe. This is especially important because the universe has undergone several other transitions *e.g.* Electroweak, GUT, etc, but among these the QCD transition is the only one which is accessible through the presently available accelerator energy. The study of the temperature fluctuation in the cosmic microwave background radiation (CMBR) originated from the recombination era (about 300,000 years after the BB) has provided crucial knowledge in supports of BB model [7, 8] and matter content of the universe. The polarization of photons due to Thomson scattering from the anisotropic decoupling surface (where the photon had suffered the last interactions) results in the non-zero quadrupole moment of the phase space distribution of the incident photon. This anisotropic fluctuations in density, for example, may be caused by the propagation of gravitational wave in the early universe. The temperature fluctuation in the CMBR is introduced as a perturbation in the phase space distribution of photons. The evolution of this perturbation is studied by using Boltzmann transport equation (BTE) [8, 9] in gravitational field. The linear polarization due to the scattering is connected with the quadrupole moment of the phase space distribution of photon.

In this work we would like to perform a theoretical analysis of LB following procedure similar to the one used in the analysis of CMBR. Study of fluctuation can be useful to characterize the state of the matter and also to put constraints on models. Power spectrum in HICRE has been discussed by several authors in Refs. [10–13]. In Ref. [10] the root mean square of various flow harmonics have been calculated and shown strong similarities with the power spectrum of CMBR. Mócsy and Sorensen [11] has extracted the power spectrum of the system produced in HICRE by using data on transverse momentum (p_T) correlations. In Ref. [13] data from ALICE collaboration has been used to estimate p_T fluctuation and subsequently expanded in Laplace series to estimate the power spectrum analogous to temperature fluctuation in CMBR. In Ref. [12] relativistic heavy ion collision events have been generated by using HIJING [14] and redistributed the produced particles to emulate flow effects to reproduce elliptic flow with required value.

The state of the matter, the QGP created in HICRE imitates the condition that prevailed in the micro-second old universe. The space time evolution of the matter is governed by fluid dynamics for both BB and LB. However, there are glaring differences too. For example, the relevant interactions, characteristic length and time scales in LB and BB are very different, primarily because of the pertinence of gravity in the BB. In HICRE there are several sources of fluctuations. Fluctuations in thermal variables have been suggested as signals of the critical end point in the QCD phase transition [15–17]. Different magnitude of fluctuations in partonic and hadronic phases in the net electric charge and baryon number may shed light on the QCD phase transition in HICRE [18]. Fluctuations in the ratio of positively to negatively charged pions may be used as an indicator of QCD transition [19] as well as for understanding the chemical equilibrium in the system formed in HICRE [20].

In the present work we will study the power spectrum due to fluctuations in the initial energy density that may arise naturally due to the quantum fluctuation of the finite "lump-like" nucleons within the colliding nuclei [21, 22]. These fluctuations evolve hydrodynamically [23–29]. The bulk matter *i.e.* QGP created in HICRE with very high temperature and pressure will expand relativistically against vacuum. This expansion is treated in the present work by solving relativistic hydrodynamic equations in (3+1) dimension with initial conditions derived from Optical as well as Monte-Carlo Glauber model [30]. The equation of state (EoS) is taken from QCD. The system will revert to hadrons due to the cooling caused by the expansion. In the hadronic phase the system may continue to expand hydrodynamically until the mean free path of the constituents become too large to maintain equilibrium. When the hadrons cease to interact, their momenta get frozen and hit the detector with that momenta. However, it has been shown that the chemical freeze-out of the hadrons takes place near the quark-hadron transition boundary, meaning that the system may be out of chemical equilibrium in the hadronic phase and the evolution of the hadronic phase can not be studied using hydrodynamics, it may require hybrid model approach (hydro+URQMD [31]) which is beyond the scope of the present work. Therefore, we will evaluate the power spectrum of the QGP phase only in this work.

We will also study the power spectrum of anisotropic fluctuations in momentum space inflicted through the phase space distribution that may drive the system slightly away from equilibrium. The evolution of such anisotropic fluctuations is dictated by the Boltzmann transport equation (BTE). The propagation of the jets through QGP may cause such fluctuations [32]. Therefore, we intend to study the evolution of the fluctuations through BTE in a hydrodynamically expanding QGP background. The BTE is solved in relaxation time (τ_R) approximation. τ_R has been taken from calculations done within the framework of hard thermal loop approximation in QCD. In principle, τ_R is a function of temperature (T) and baryonic chemical potential (μ_B), however, as discussed below in the present case we need to consider the T dependence only. The change in T due to expansion of the bulk is controlled by relativistic hydrodynamics. This change in T affects evolution of the fluctuation (solution of the BTE) through the relaxation time, indicating a direct coupling between the anisotropic fluctuation and bulk expanding background. The BTE has been solved with initial conditions containing spatial anisotropies to be specified later.

The initial energy density distribution, $\epsilon(\tau, x, y, \eta)$ of the bulk matter created in HICRE can be estimated by using Glauber model. In the present work, both the Optical Glauber (OG) as well as the Monte-Carlo Glauber (MCG) models are used to demonstrate the sensitivity of the results on initial conditions of the bulk matter. The finite size of the colliding nucleons with quantum fluctuations in the nuclear beams will create "lumpiness" in $\epsilon(\tau, x, y, \eta)$. This can be seen very clearly in $\epsilon(\tau, x, y, \eta)$ calculated using MCG. We study the evolution of these fluctuations using hydrodynamics at the surfaces of constant T . Power spectrum due to fluctuations caused by phase space perturbations has also been estimated.

In the present work we make an attempt to evaluate the fluctuations in HICRE in keeping close resemblance with analysis of temperature fluctuation in cosmic microwave radiation (CMBR). The power spectrum will be evaluated at various stages of the evolving system to understand how it changes with time.

The paper is organized as follows. In the next section we will briefly discuss the evolution of the quark gluon plasma within the framework of relativistic hydrodynamics followed by discussions on the initial conditions and equation of state used in this work in the successive subsections. In section III the evolution of the fluctuations within the ambit of Boltzmann Transport Equation (BTE) has been discussed. The power spectrum has been evaluated in section IV. Section V is devoted to present the results and section VI is dedicated to summary and discussions.

II. HYDRODYNAMIC EVOLUTION OF THE QUARK GLUON PLASMA

The expansion of the QGP in space and time can be described by applying relativistic hydrodynamics. The conservation of energy and momentum of the fluid is governed by the equation:

$$\partial_\mu T^{\mu\nu} = 0 \quad (1)$$

where $T^{\mu\nu} = (\epsilon + P)u^\mu u^\nu - g^{\mu\nu}P$. Here ϵ is the energy density, P is the pressure, $u^\mu = \gamma(1, \vec{v})$ is the four velocity of the fluid and $\gamma = 1/\sqrt{1-v^2}$. The conservation of the net baryon number throughout the evolution history is controlled by the equation:

$$\partial_\mu (n_B u^\mu) = 0 \quad (2)$$

where n_B is the net baryon (baryon - antibaryon) density. In the present work we are interested in the system produced in nuclear collisions at highest RHIC energies where n_B is negligibly small (n_B will be even smaller at LHC collision conditions) and hence $\mu_B \sim 0$. Therefore, we do not need to consider Eq. 2. In the present work Eq. 1 has been solved numerically using standard technique [33] in full (3+1) space-time dimension without assuming boost invariance along longitudinal direction [34] and cylindrical symmetry of the system. The initial conditions and equation of state (EoS) used here are discussed briefly below.

A. Initial conditions

The initial conditions required to solve Eq. 1 in (3+1) dimension are as follows: The Cartesian components of initial flow velocities are: $v_x(\tau_0, x, y, z) = v_y(\tau_0, x, y, z) = 0$ and the initial energy density profile is taken as [33]:

$$\varepsilon(\tau_0, x, y, \eta_s) = \varepsilon_{GM}(x, y) \theta(Y_b - |\eta_s|) \exp \left[-\theta(|\eta_s| - \Delta\eta) \frac{(|\eta_s| - \Delta\eta)^2}{\sigma_\eta^2} \right] \quad (3)$$

where $\varepsilon_{GM}(x, y)$ is obtained from OG or MCG model, having the following expression

$$\varepsilon_{GM}(x, y) = \varepsilon_0 \left[\frac{1-f}{2} n_{part}(x, y) + f n_{coll}(x, y) \right] \quad (4)$$

We have taken the value of the inelastic nucleon-nucleon cross section at RHIC energy as, $\sigma_{NN} = 42$ mb in evaluating the number of participants, n_{part} and number of collisions, n_{coll} . In MCG model approach the energy density is deposited at discrete points, but for hydro evolution we need a continuous distribution of energy density. Therefore, we use Gaussian smearing to get the energy density as:

$$\varepsilon_{GM}(x, y) = \frac{1}{2\pi\sigma^2} \sum_i \varepsilon_{GM}(x_i, y_i) e^{-\frac{(x-x_i)^2 + (y-y_i)^2}{2\sigma^2}} \quad (5)$$

where $\varepsilon_{GM}(x_i, y_i)$ is obtained from Eq(4). To sample the nucleons from nuclei (Au in this case), we use the following Woods-Saxon distribution

$$\rho(r) = \frac{\rho_0}{1 + e^{\frac{r-R}{\delta}}}$$

The values of different parameters appeared in the above expressions are tabulated below.

Parameter	Value
τ_0	0.6 fm/c
Y_b	5.3
$\Delta\eta$	1.3
σ_η	2.1
ε_0	7.7 GeV/fm ³
f	0.14
σ^2	0.16
R	6.37
δ	0.535
σ_{NN}	42 mb

B. Equation of State (EoS)

The EoS for the QGP and the hadrons have been constructed following the procedure outlined in Ref [35]. We use excluded volume model [36] for hot hadrons and pQCD results [35, 37, 38] for the QGP phase. For a smooth crossover, a switching function is used as in [35] and the parameters are adjusted so as to match the Lattice QCD results. A brief description of the model used is as follows. We choose volume of hadrons to be proportional to mass, $v_i = m_i/m_0$ as in [35], where m_0 is a constant. We take $m_0 = 0.9$ for this work. The pressure of the hadronic medium is taken to be

$$p_{HG}(T, \mu_B) = \sum_{i=1} p_i^{id}(T, \tilde{\mu}_i) \quad (6)$$

$$\tilde{\mu}_i = \mu_i - v_i p_{HG} \quad (7)$$

where $\mu_i = B\mu_B$ and B is baryon number. p_i^{id} denotes the ideal pressure of a relativistic gas comprised of i^{th} resonance and p_{HG} is the pressure after excluded volume correction is taken into account which is found by solving the above set of equations in a self-consistent way.

The pressure of the QGP phase is taken as

$$P = \frac{8\pi^2}{45} T^4 \left[f_0 + \left(\frac{\alpha_s}{\pi}\right) f_2 + \left(\frac{\alpha_s}{\pi}\right)^{3/2} f_3 + \left(\frac{\alpha_s}{\pi}\right)^2 f_4 + \left(\frac{\alpha_s}{\pi}\right)^{5/2} f_5 + \left(\frac{\alpha_s}{\pi}\right)^3 f_6 \right] \quad (8)$$

where the coefficients f_n 's are given in the appendix A. The coupling, α_s has been taken from [40] calculated in three loop approximations. The pressure in the crossover region is taken to be

$$P(T, \mu) = S(T, \mu) P_{qgp}(T, \mu) + (1 - S(T, \mu)) P_h(T, \mu) \quad (9)$$

where the switching function $S(T, \mu)$ is taken as

$$S(T, \mu) = \exp\{-\theta(T, \mu)\} \quad (10)$$

$$\theta(T, \mu) = \left[\left(\frac{T}{T_0}\right)^r + \left(\frac{\mu}{\mu_0}\right)^r \right]^{-1} \quad (11)$$

We take $T_0 = 165$ MeV, $\mu_0 = 3\pi T_0$ and $r = 4$. With these parameter values we find a good agreement of our results with the lattice data [41].

III. EVOLUTION OF ANISOTROPIES AND FLUCTUATIONS

In this section, we discuss the connection of δf , a small deviation in phase space distribution from its equilibrium value with the fluctuations in various thermodynamic quantities. The phase space distribution function, $f(\vec{x}, \vec{p}, t)$ of a system slightly away from equilibrium, at time t , position \vec{x} , momentum \vec{p} can be written as [42]: $f(x, p) = f_0(x, p) + \delta f(x, p)$ with $\delta f = f_0 \psi$. The evolution of δf is governed by the BTE, $p^\mu \partial_\mu f = (p \cdot u) C[f]$ [42–44]. For an expanding system under the relaxation time approximation BTE reduces to the following (see [45] for details) [46–51]:

$$\left(\frac{\partial}{\partial t} + \frac{\vec{p}}{p^0} \cdot \frac{\partial}{\partial \vec{x}} + \frac{(p^0 u_0 - \vec{p} \cdot \vec{u})}{p^0 \tau_R(x)} \right) \delta f(x, p) = - \left(\frac{\partial}{\partial t} + \frac{\vec{p}}{p^0} \cdot \frac{\partial}{\partial \vec{x}} \right) f_0(x, p) \quad (12)$$

Eq. 12 can be solved by using standard techniques used for partial differential equations [52]. The solution is given by:

$$\delta f(x, p) = D(t, t_0) \left[\delta f_{in}(p, \vec{x} - \frac{\vec{p}}{p^0}(t - t_0)) + \int_{t_0}^t B(\vec{x} - \frac{\vec{p}}{p^0}(t - t'), t') D(t_0, t') dt' \right] \quad (13)$$

where $D(t_2, t_1)$ is given by,

$$D(t_2, t_1) = \exp \left[- \int_{t_1}^{t_2} dt' A(p, \vec{x} - \frac{\vec{p}}{p^0}(t' - t_0), t') \right] \quad (14)$$

with

$$A(p, \vec{x}, t) = \frac{p^0 u_0(x) - \vec{p} \cdot \vec{u}(x)}{p^0 \tau_R(x)} \quad (15)$$

and

$$B(\vec{x}, t) = - \left(\frac{\partial}{\partial t} + \frac{\vec{p}}{p^0} \cdot \frac{\partial}{\partial \vec{x}} \right) f_0(x, p). \quad (16)$$

In equilibrium, f_0 is given by:

$$f_0(x, p) = \frac{1}{e^{\beta(x)(u^\mu p_\mu) \pm 1}} \quad (17)$$

for which the expression for B reduces to:

$$B(\vec{x}, t) = -f_{eq}(1 + f_{eq}) \frac{p^\mu}{p^0} \partial_\mu [\beta(x) u^\mu p_\mu] \quad (18)$$

where $\beta = 1/T(x)$, $u^\mu(x) = (\gamma, \gamma \vec{v})$ is the flow velocity of the fluid and the Lorentz factor is given by, $\gamma(x) = u^0(x) = (1 - v(x)^2)^{-1/2}$. The space time dependence of T and \vec{v} are determined by the solution of the hydrodynamic equations.

Once δf is known perturbations in various thermodynamic quantities *e.g.* in energy density (ϵ), entropy density (s), temperature etc can be obtained as follows. Any deviation from the equilibrium value in the thermodynamic quantities may be incorporated through the deviation in the distribution function. As discussed the distribution function may be written as:

$$f(\vec{x}, \vec{p}, t) = f_0(p) \{1 + \Psi(\vec{x}, \vec{p}, t)\}, \quad (19)$$

The energy-momentum tensor ($T^{\mu\nu}$) of the system may be expressed in terms of f as follows:

$$T^{\mu\nu} = \int d^3p \frac{p^\mu p^\nu}{p^0} f^{(0)}(p) \{1 + \Psi(\vec{x}, \vec{p}, t)\}. \quad (20)$$

where $T^{\mu\nu}$ can be split into equilibrium part ($\overline{T}^{\mu\nu}$) and a deviation, $\Delta T^{\mu\nu}$ from the equilibrium value *i.e.* $T^{\mu\nu} = \overline{T}^{\mu\nu} + \Delta T^{\mu\nu}$. The tensor $T^{\mu\nu}$ can be decomposed into various components in terms of thermodynamic quantities as:

$$\begin{aligned} T_0^0(x_i, t) &= -\{\epsilon + \delta\epsilon(x_i, t)\}, \\ T_i^0(x_i, t) &= -T_0^i = (\epsilon + P)u_i, \\ T_j^i(x_i, t) &= \{P + \delta P(x_i, t)\}\delta_j^i + \Sigma_j^i(x_i, t), \\ \Delta T_i^i &= 0, \end{aligned} \quad (21)$$

where P is the average pressure, u_i is the i^{th} spatial component of the flow velocity and Σ_j^i is the stress tensor which contains the shear viscous coefficient (see [45] for details). The evolution of the flow velocity, energy density, pressure, temperature etc can be obtained from the solution of hydrodynamic equations. The interaction of the expanding background (hydrodynamics) with the perturbations (δf) at each space-time point is enforced through temperature (appearing through τ_R) and flow velocity which are obtained from the solution of the relativistic hydrodynamic equations. Therefore, the fluctuations represent interaction between equilibrium (hydrodynamics) and non-equilibrium (BTE) degrees of freedom.

The formalism discussed above can be used to any system where the fluctuations are evolving in an expanding background aided by: (a) initial distribution δf_{in} appearing in Eq. 13, (b) τ_R which is determined by the interaction at the microscopic level, (c) flow velocity and temperature determined by the solutions of hydrodynamic equations which needs inputs like initial energy density and velocity distributions as well as EoS controlled by the interactions in the system under study.

In the present work we will apply this formalism to the system formed in HICRE. Therefore, we will use QCD based calculations for estimating $\tau_R(T)$ as: $\tau_R^{-1}(x) = 1.1\alpha_s T$ performed in Ref. [53] in HTL (Hard Thermal Loop approximation).

The power spectra have been evaluated for the following two scenarios: (i) for the fluctuation in the initial conditions within the ambit of OG and MCG models through the initial energy density profile, (ii) for fluctuations caused by perturbations in phase space distribution. The latter one has been evolved through BTE in an expanding thermal QGP background. To simulate different types of initial spatial anisotropy one may choose,

$$\delta f(p, \vec{x}, t_0) = A_0 \exp[-r(1 + a_n \cos n\vartheta)] \quad (22)$$

where A_0 is a constant and n can be taken as $n = 2, 3, 4, 5, \dots$ to simulate different geometry for the initial anisotropy (see also [11]). We have taken $A_0 = 1$ and set the perturbation centered around $r = 0$ here.

IV. THE POWER SPECTRUM

We are now equipped to study the evolution of the power spectrum of the angular distribution of particles which originates due to: (i) fluctuations in initial energy density profile evaluated in OG and MCG models by using the momentum distributions of particles at various surfaces of constant temperatures with the help of mathematical expression given in [54]:

$$E \frac{dN_0}{d^3p} = \frac{g_i}{(2\pi)^3} \int_{\Sigma} d\sigma_{\mu} p^{\mu} f_0(x, p) \quad (23)$$

where $d\sigma_{\mu}$ is the surface element, p^{μ} is the 4-momenta of the particle and in Milne coordinate these are expressed as follows [33, 55]:

$$\begin{aligned} d\sigma_{\mu} &= (\tau_f dx_f dy_f d\eta_f, -\tau_f d\tau_f dy_f d\eta_f, -\tau_f d\tau_f dx_f d\eta_f, -\tau_f d\tau_f dx_f dy_f) \\ &= \left(1, -\frac{\partial\tau_f}{\partial x_f}, -\frac{\partial\tau_f}{\partial y_f}, -\frac{\partial\tau_f}{\partial\eta_f}\right) \tau_f dx_f dy_f d\eta_f \\ p^{\mu} &= (m_T \cosh(y - \eta_f), p_x, p_y, m_T \sinh(y - \eta_f)/\tau_f) \end{aligned}$$

where η_f is the fluid rapidity, τ_f is the proper time, x_f and y_f are transverse coordinate for the fluid. p_x, p_y are the fluid momenta in Cartesian coordinate, y is the particle rapidity and $m_T = \sqrt{p_T^2 + m^2}$ is the transverse mass of the particle. In the above equation subscript f stands for fluid. Therefore,

$$p^{\mu} d\sigma_{\mu} = \left[m_T \cosh(y - \eta_f) - p_x \frac{\partial\tau_f}{\partial x} - p_y \frac{\partial\tau_f}{\partial y} - \frac{m_T \sinh(y - \eta_f)}{\tau_f} \frac{\partial\tau_f}{\partial\eta_f} \right] \tau_f dx_f dy_f d\eta_f$$

For massless particles, y is given by

$$y = -\ln \left[\tan \left(\frac{\theta}{2} \right) \right]$$

which is same as the pseudo-rapidity (η) of the particle.

(ii) Similarly the fluctuation in the particle distribution due to the perturbation, δf in phase space distribution obtained within the framework of relaxation time approximation by solving BTE in an expanding QGP background. δf can be used to estimate perturbations thermodynamic quantities as mentioned earlier. We use $f = f_0 + \delta f$ to estimate the p_T distribution of particles away from equilibrium as:

$$E \frac{dN}{d^3p} = \frac{g_i}{(2\pi)^3} \int_{\Sigma} d\sigma_{\mu} p^{\mu} [f_0 + \delta f(x, p)] \quad (24)$$

Now the quantities, EdN_0/d^3p or EdN/d^3p can be expanded in Laplace series in terms of spherical harmonics, $Y_{lm}(\theta, \phi)$ at a given transverse momentum (p_T) and temperature. We identify pseudo-rapidity, η as the polar angle, $\eta = -\ln\{\tan(\theta/2)\}$.

The power spectrum of the fluctuations in the transverse momentum (p_T) distribution of particles can be estimated at surfaces of constant temperatures to understand how the power spectrum changes as the system cooled down with the progression of time. The power spectrum of EdN/d^3p can be estimated as follows:

$$E \frac{dN}{d^3p} = \bar{N} + \sum_{l=1}^{\infty} \sum_{m=-l}^l a_{lm}(p_T, T) Y_{lm}(\theta, \phi) \quad (25)$$

where

$$\bar{N} = \frac{1}{4\pi} \int d\Omega \frac{dN}{d^2p_T dy} \quad (26)$$

the coefficients, a_{lm} 's are determined as follows:

$$a_{lm}(p_T, T) = \int d\Omega Y_{lm}^* E \frac{dN}{d^3p} \quad (27)$$

For determining power spectrum without perturbation we replace EdN/d^3p by EdN_0/d^3p in Eq. 27. The terms in Eq. 25 with different l corresponds to different angular scales: terms with larger l will have smaller angular resolution. The angular resolution $\theta_r = \pi/l$ [8] determines the value of the maximum l i.e. l_{max} . For heavy ion experiments at RHIC and LHC the resolution in pseudo-rapidity will govern the value of l_{max} .

Using standard techniques and properties of spherical harmonics, the angular power spectrum (C_l) of EdN/d^3pJ can be written as:

$$C_l(p_T, T) = \frac{1}{2l+1} \sum_m |a_{lm}|^2 \quad (28)$$

indicating the distribution of power of fluctuations among different angular scales determined by l . In CMBR fluctuation, C_l for the temperature fluctuation, $\Delta T(\theta, \phi)/T$ has been calculated theoretically and compared with experimental data which has enhanced our understanding on the matter content of the universe. The power spectrum, C_l 's are related to the various flow harmonics [56–61] and the relation is derived in appendix B. In analogy with CMBR, the solution of BTE can be used to estimate the fluctuations in temperature ($\Delta T/T$),

$$\frac{\Delta T}{T} = - \left(\frac{\partial \ln f_0}{\partial \ln p} \right)^{-1} \Psi \quad (29)$$

V. RESULTS

We have solved the (3+1) dimensional relativistic ideal hydrodynamic equations with initial conditions (due to OG and MCG models) and EoS described above to study the evolving QGP. The Boltzmann transport equation has been solved in relaxation time approximation in this expanding background to study the effects of phase space perturbation. The solution of BTE can be used to estimate the power spectrum due to phase space perturbations in various physical quantities. We present the results for the following two sets of conditions:

(i) The power spectrum of EdN_0/d^3p due to fluctuations in initial energy density- we estimate the power spectrum and its evolution of the p_T distributions of particles ($dN_0/d^2p_T dy$) for OG and MCG model initial conditions at surfaces of constant temperatures. We will evaluate the power spectrum at $T = 350$ MeV which is close to the initial temperature, at the transition temperature (T_c), $T = T_c = 170$ MeV and at some intermediary temperature, $T = 250$ MeV to understand how the power spectrum evolve from the initial to the transition point.

(ii) Power spectrum of EdN/d^3p which contains the perturbations has been estimated. The perturbation in phase space has been obtained from the solution of BTE.

First we consider (i): in Fig. 1 the initial energy density profile due to OG model is displayed for central Au + Au collision at $\sqrt{s_{NN}} = 200$ GeV. The thermalization time has been taken as $\tau_i = 0.6$ fm/c. Other parameters regarding the initial condition are displayed in table I in section V. The profile evaluated at zero space-time rapidity has isotropic symmetry with sharp fall near the boundaries. In Figs. 2 and 3, the surfaces of constant temperatures evolved hydrodynamically for initial energy density (shown in Fig. 1) have been depicted. Fig. 2 (Fig. 3) shows the result for $T = 350$ (170) MeV. We observe no qualitative change in the shape of the surfaces except at lower temperature the space-time size of the surface becomes larger. It is important to note that the energy density profile and consequently the constant temperature surfaces are smooth - not showing any distinct fluctuations because of the absence of fluctuation in the initial energy density profile in OG model.

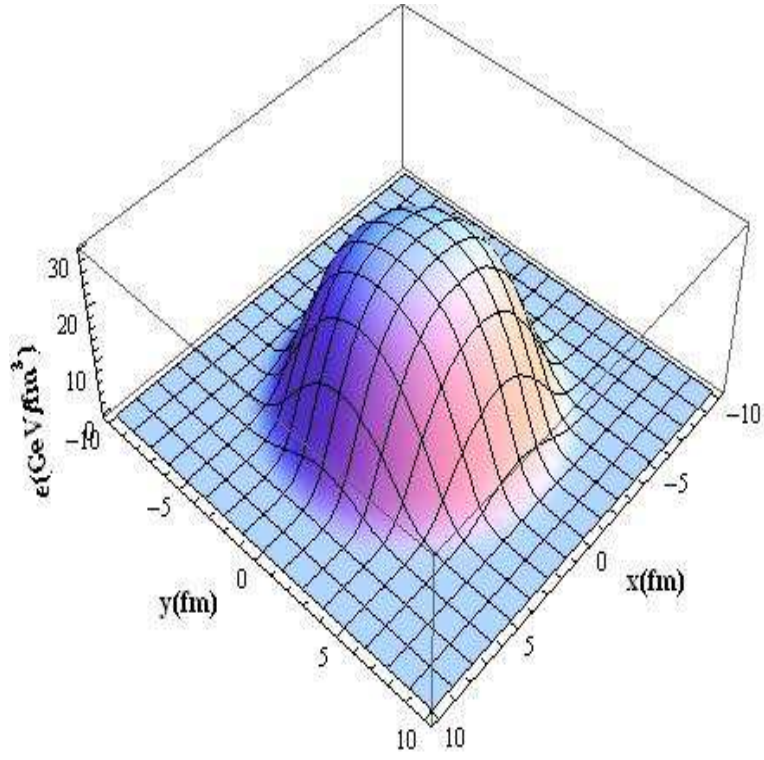


FIG. 1: Initial energy density profile in the transverse plane at space time rapidity = 0 in the OG model for Au+Au central collision.

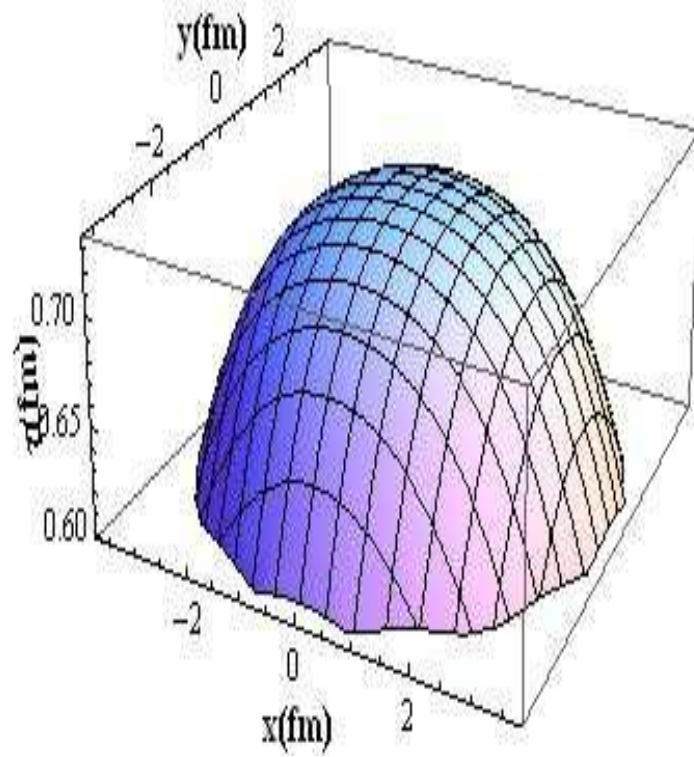


FIG. 2: The constant temperature, $T = 350$ MeV surface in the time-transverse plane.

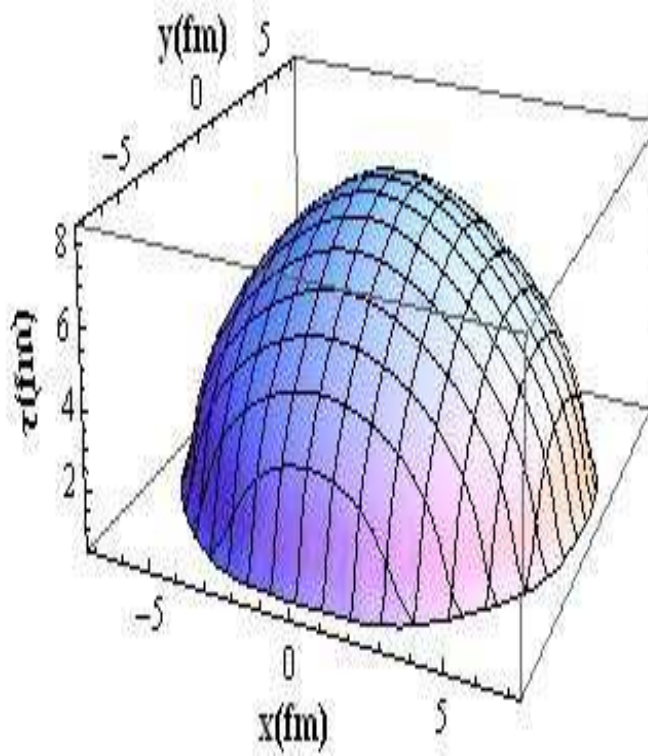


FIG. 3: The constant temperature surface in the time-transverse plane for 170 MeV.

Similar to the OG initial condition we plot the initial energy density profile evaluated in MCG model for 0–5% centrality collision of Au + Au at $\sqrt{s_{NN}} = 200$ GeV in Fig. 4 with $\tau_0 = 0.6$ fm. We observe lumpiness of complicated nature in the initial energy density profile at various position in the transverse plane due to the collisions of nucleons with fluctuating positions in the colliding beam nuclei.

The constant temperature surface at $T = 350(250)$ MeV is displayed in (τ, x, y) coordinate in Fig. 5 (Fig. 6) for MCG initial condition. It is observed that the initial energy density has significant fluctuations in space time coordinate. These inhomogeneities will create pressure imbalance with the neighbouring zones - higher density domains will exert larger pressure and hence will expand faster to smoothen the inhomogeneities. As a result the inhomogeneity will reduce and their distributions will change. We observe that the size of the surface in space-time coordinate has increased at lower temperature. The large fluctuations at the surface corresponding to $T = 350$ MeV resulting from the inhomogeneities in the initial energy density profile have reduced in magnitude at the $T = 250$ MeV surface as the system evolve hydrodynamically. The domains of high energy densities (Fig. 4) will take longer time to reach a given temperature as can be seen from Fig. 5 where for certain domains τ is larger compared to others. The constant temperature surface ($T = 170$ MeV, say) is defined here as $T(x, y, \tau, \eta_s = 0) = 170 \text{ MeV}$ where η_s is space-time rapidity. This will give $\tau = \tau(x, y)$. We observe that the differences in the values of $\tau(x, y)$ at various points in $x - y$ plane is smaller in the $T = 170$ MeV surface than at $T = 350$ or 250 MeV surfaces. Indicating that the system is approaching toward a homogeneous one in coordinate space and through expansion this inhomogeneities get transferred to momentum space.

In Fig. 8 the η (upper panel) and θ (lower panel) distributions of particles have been displayed at the surface of constant temperatures, $T = 350$ MeV. We find that the fluctuations in differential particle numbers is larger at MCG than OG model, which is clearly visible both in the η and θ distributions. However, with progress in time or with the reduction of temperature at $T = 170$ MeV (Fig. 9) the total number of particles increase and more particles appear at larger η enhancing the width of the distributions. The θ distribution shows a plateau over a larger domain of θ

Next we would like to study - how the power spectrum of the fluctuations caused by initial energy density profiles evolve. We will study the power spectrum of particle spectra, EdN_0/d^3p at the surfaces of constant temperatures at $T = 350, 250$ and 170 MeV. The angular distribution of particles at constant p_T has been analyzed by decomposing it in terms of spherical harmonics as discussed in section IV.

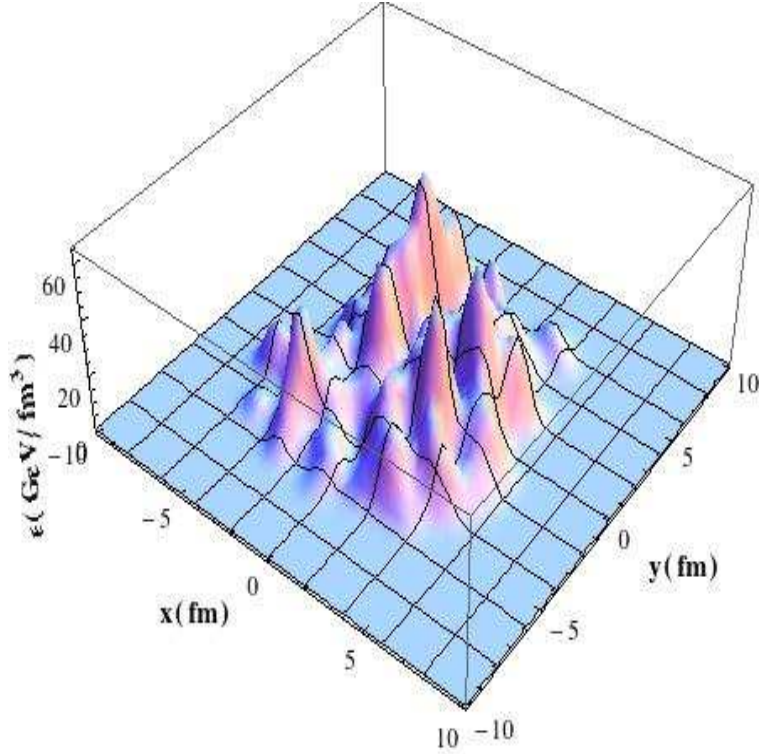


FIG. 4: Same as Fig. 1 with MCG initial condition.

The power spectrum of the distribution, C_l has been plotted in Fig. 10 for the angular distribution of the spectra at $T = 350$ MeV for the OG initial condition. We clearly find that the power spectrum corresponding to the odd l 's are negligibly small because the distribution is an even function of θ .

In Figs. 11 and 12 the power spectrum for the angular distribution at the the surface of $T = 250$ and 170 MeV respectively have been depicted. We observe that there is no significant change in the power spectrum for the OG initial conditions at lower temperatures. With time, the spatial inhomogeneities in $x - y$ plane (which are translated into momentum space) of the system gets reduced as the system favours to erase out any pressure imbalance, however, for systems without fluctuation as in OG case, does not show much change. In case of OG initial conditions the system is symmetric, (Fig. 1) therefore, with the evolution from higher to lower temperatures (Fig. 2 and 3) there is no significant change in the power spectrum.

However, for MCG initial condition, the system is highly inhomogeneous (Fig. 4). The pressure gradients caused by the inhomogeneity acts in favour of reducing it (Fig. 5 and 7) during the course of expansion from higher to lower temperature. Therefore, it is clearly seen that the power spectrum of the system appears to be different at $T = 250$ MeV as the contribution from odd l are enhanced compared its value at $T = 350$ MeV. We also note that quantitatively, C_l 's increases with lowering of temperatures both for OG and MCG initial conditions (see later). It is well known that smaller (larger) l 's resolve larger (smaller) angular anisotropy. The value of l sets the angular scale (θ_l) as: $\theta_l = \pi/l$. The most interesting aspect is that at lower temperatures ($T = 170$ MeV), the power spectrum at odd l 's so becomes comparable in magnitude to the values at even l 's. The enhancement of the odd l 's is an indicator of the presence of inhomogeneities in the initial condition. The enhancement of C_l 's for large l at lower temperature ($T = 170$ MeV) indicates appearance of lower smaller angular fluctuations.

(ii) So far we have discussed the evolution of power spectrum created in the initial collision dynamics. However, fluctuations represented by δf may be caused by other sources also, *e.g.* propagation of jets through the medium may create such fluctuations. Therefore, next we make some case studies on the propagation of fluctuations by introducing perturbations $\delta f(\vec{p}, \vec{x}, t)$ in phase space distribution by solving BTE in expanding background. In Fig. 13 the initial perturbation δf (Eq. 22 for $n = 2$) has been displayed. We study the power spectrum of $E d\delta N/d^3p$ for the perturbation shown in Fig. 13. The power spectrum, C_l at $T = 350, 250$ and 170 MeV, for both OG and MCG are depicted in Figs. 14, 15 and 16 for $p_T = 0.6$ GeV. We recall that there is no inhomogeneity in OG initial condition. Therefore, this study gives us an opportunity to learn

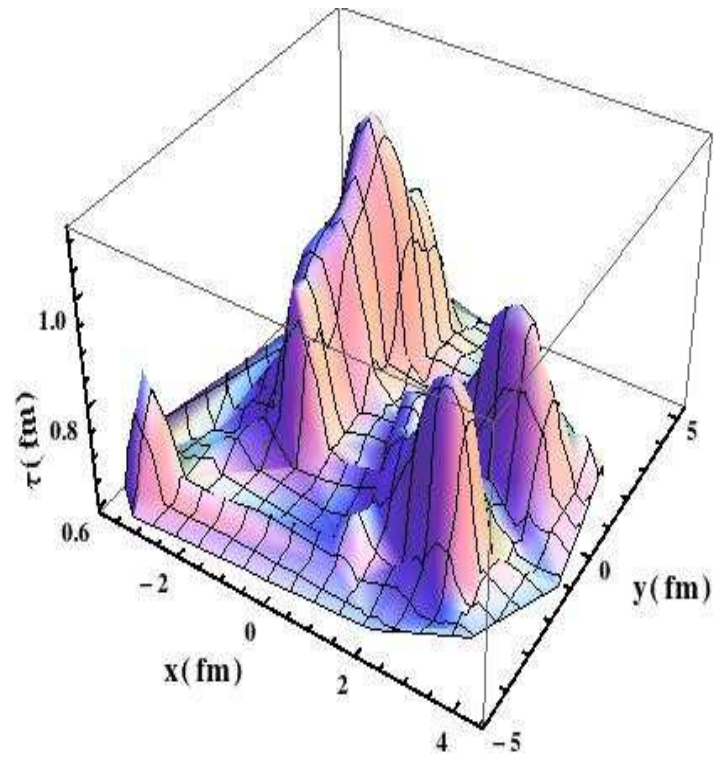


FIG. 5: The constant temperature surface at $T = 350$ MeV for MCG initial condition.

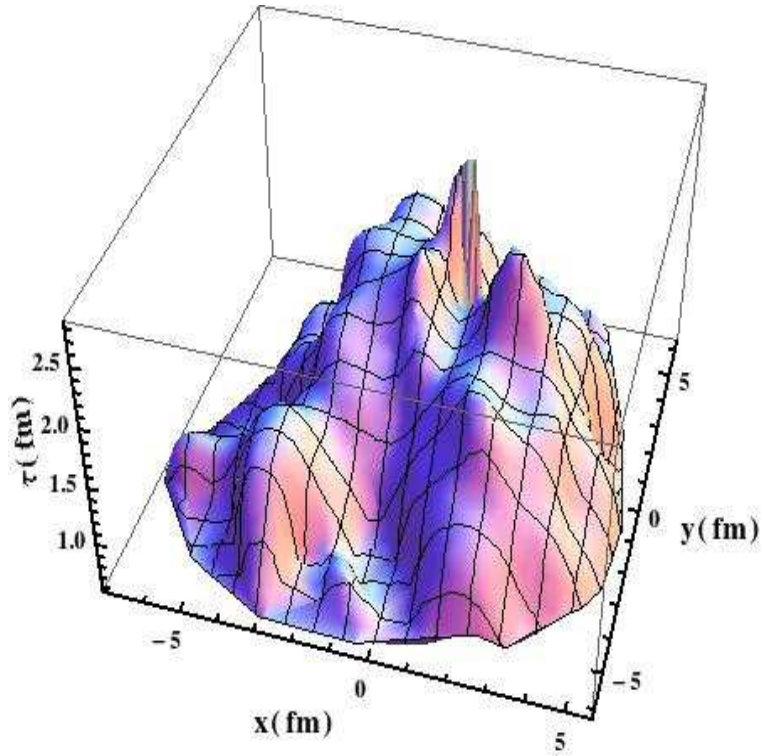


FIG. 6: Same as Fig. 5 for MCG initial condition at $T = 250$ MeV.

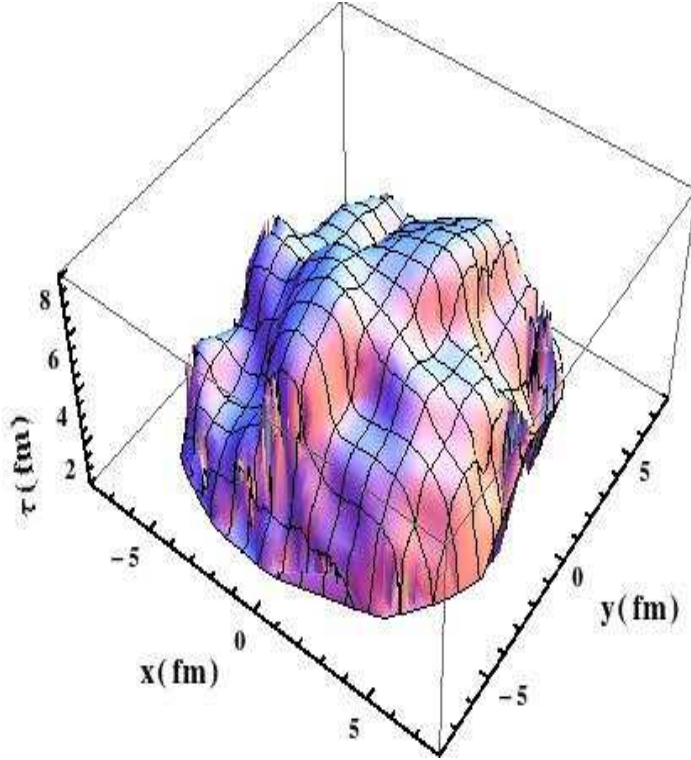


FIG. 7: Same as Fig. 5 at $T = 170$ MeV.

how the local fluctuations (due to δf) evolve with the expanding background inhomogeneities. We find that the spectrum with OG initial condition remains largely unaltered. However, the amplitude of the spectrum with MCG initial conditions changed significantly. The crucial point to be noted here is that the magnitude of the power spectrum with the perturbation is much larger than the spectrum derived from the MCG initial condition (with $\delta f = 0$). For $\delta f \neq 0$ the magnitude of power spectrum for even l is dominant over its odd counter parts at $T = 170$ MeV in contrast to the case with $\delta f = 0$ where the difference in the values of C_l between odd and even l is small. This is because the perturbation δf for $n = 2$ has a symmetry under the exchange $\theta \leftrightarrow -\theta$ indicating the dominance of even l through spherical harmonics. Therefore, dominance of even l in this particular case indicate the presence of perturbations.

The power spectrum with perturbation at $p_T = 1.5$ GeV are displayed in Figs. 17, 18 and 19. The amplitude of the spectrum is larger at all temperatures compared to the case with $p_T = 0.6$ GeV. Qualitatively the spectra is similar to the values at lower p_T (0.6 GeV). We find significant enhancement at odd l . The variation of power spectrum with T for different l has been displayed in Fig. 20. The C_l 's for small l decrease with T monotonically at low T and reach a plateau at higher T . The C_l 's for larger l does not show much variation with T . Similar quantities have been depicted in Fig. 21 for MCG initial condition. The fall is faster in case of MCG initial conditions. In Fig. 22 the variation of power spectrum with T for odd l has been depicted. We clearly observe that the C_l falls faster with T as compared to even l . Now we discuss the T variation of power spectrum with inclusion of perturbation (δf) for even l (the values with odd l 's are very small). In Fig. 23 (Fig. 24) the C_l is plotted as a function of temperature for $p_T = 0.6$ GeV for OG (MCG) initial condition. We observe the following features: for a given l the value of C_l 's are larger in MCG than OG initial condition, for large $l (\geq 8)$ the C_l 's do not vary significantly with T most significantly and the variation with T is non-monotonic. Similar studies have been made for higher $p_T = 1.5$ GeV. The results are shown in Figs. 25 and 26. The values of C_l 's are much larger but the qualitative behaviour is same as lower p_T for both the initial conditions. The important point to be noted here is that the nature of the power spectrum on the constant temperature surfaces with perturbation is distinctly different from the spectrum obtained without perturbation.

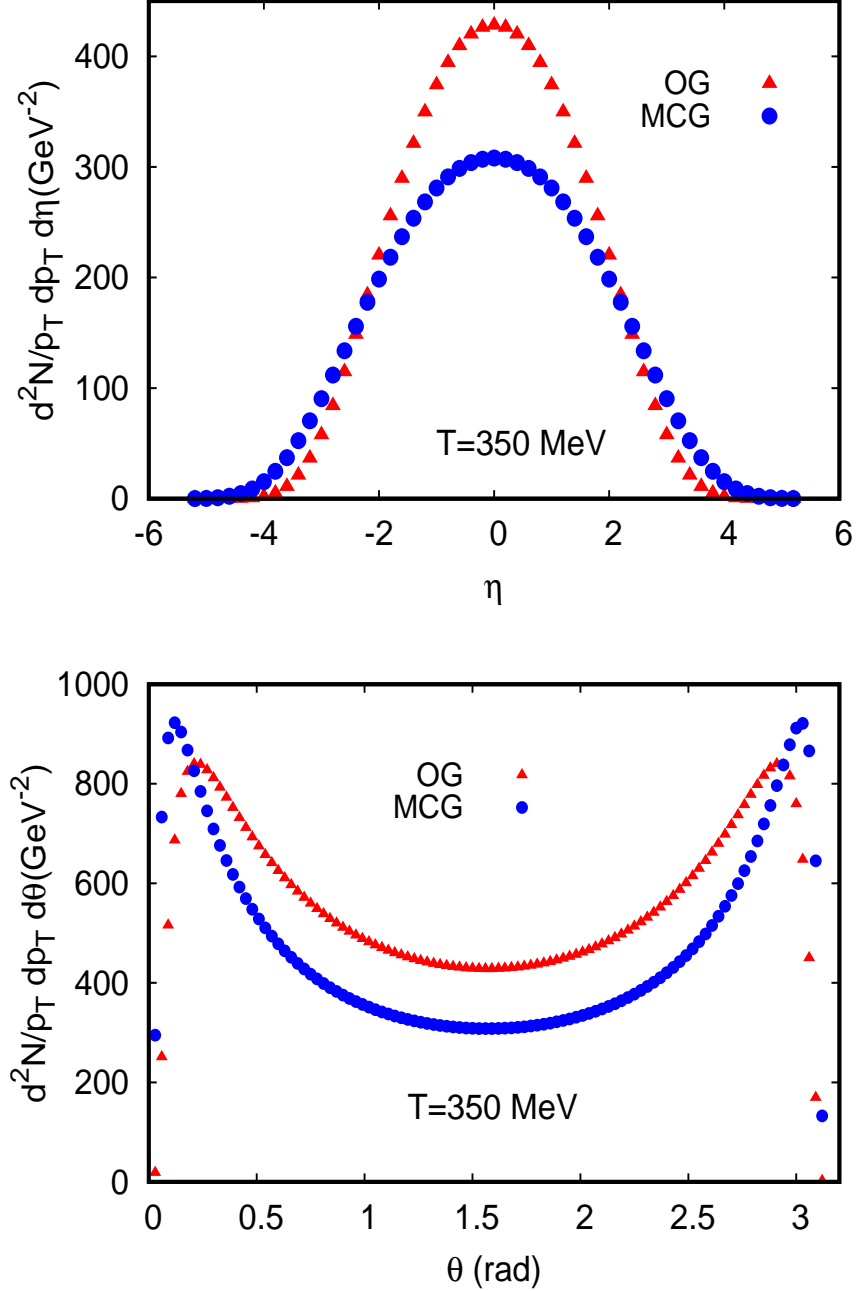


FIG. 8: The pseudo-rapidity (η) and angular (θ) distribution of particles at $p_T = 0.6 \text{ GeV}$ with OG and MCG initial conditions at $T = 350 \text{ MeV}$.

A. Relation between flow harmonics and power spectrum

The η and p_T dependence of various flow harmonics can be calculated from the power spectrum using the following relation (see appendix B for derivation):

$$2\pi \frac{dN}{p_T dp_T dy} v_k = \sum_{l \geq k}^{\infty} \sqrt{\frac{2l+1}{4\pi} \frac{(l-k)!}{(l+k)!}} [a_{l,k} + (-1)^k a_{l,-k}] P_l^k(\cos \theta)$$

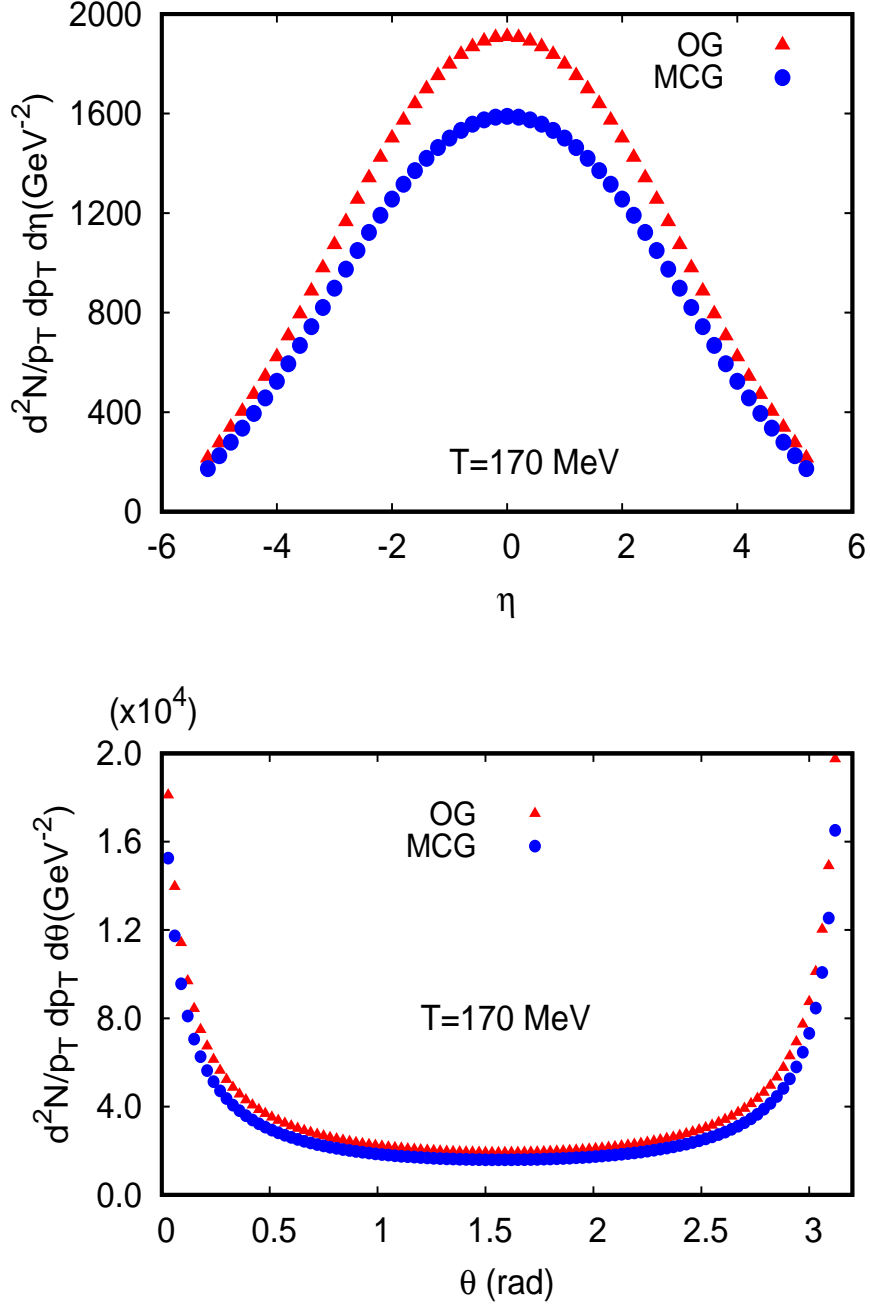


FIG. 9: Same as Fig. 8 at $T = 170 \text{ MeV}$.

For example, the elliptic flow can be calculated by using values of P_l^k as:

$$v_2 = \left(\frac{dN}{2\pi p_T dp_T dy} \right)^{-1} \text{sech}^2 \eta [a'_{22} + a'_{32} \tanh \eta + a'_{42} (7 \tanh^2 \eta - 1) + \dots] \quad (30)$$

where

$$a'_{22} = \frac{1}{3} \sqrt{\frac{5}{12\pi}} a_{22}, \quad a'_{32} = 15 \sqrt{\frac{7}{120\pi}} a_{32}, \quad a'_{42} = \frac{15}{2} \sqrt{\frac{1}{40\pi}} a_{42}, \quad (31)$$

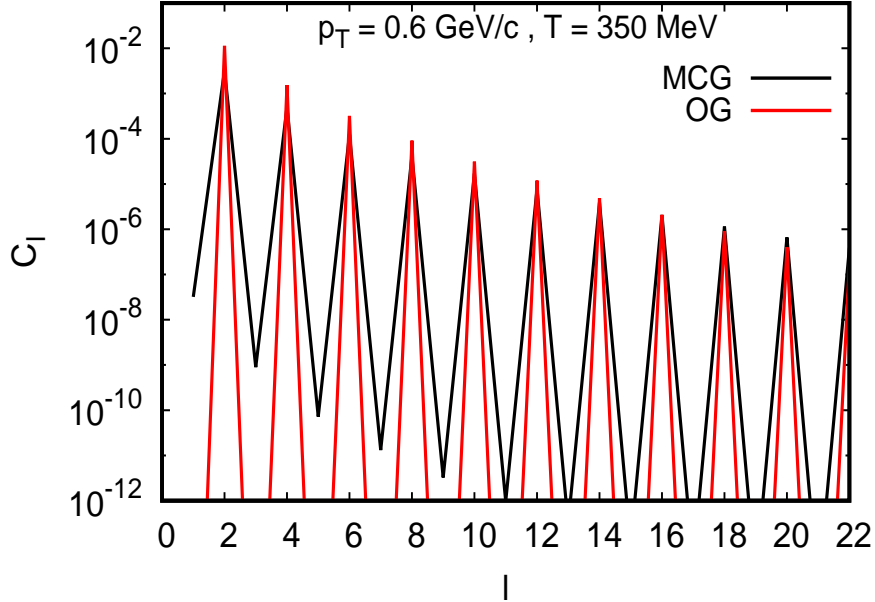


FIG. 10: The power spectrum, C_l deduced from $dN/d^2p_T dy$ at $p_T = 0.6$ GeV for both the OG and MCG initial conditions analyzed at the surface of $T = 350$ MeV.

where a_{lm} is a function of p_T and given by Eq. 27. The fluctuations in v_2 and its dependence on kinematic variables can also be estimated from the analysis of $E d\delta N/d^3p$ presented here. The fluctuations of other harmonics and its dependence on p_T , η can also be calculated using similar procedure.

VI. SUMMARY AND DISCUSSIONS

The hot and dense system formed in heavy ion collisions at relativistic energies has been evolved using (3+1) dimensional relativistic hydrodynamics. The initial energy density profiles required to solve the hydrodynamics has been derived from OG and MCG models. The power spectrum of momentum distribution of particles due to fluctuations in initial conditions for both OG and MCG models have been estimated at different surfaces of constant temperatures following the analysis procedure that has been used for CMBR spectrum. This enable us to study the evolution of the power spectrum with decrease in temperature and hence effectively with increase in time. We observe that the power spectrum with OG initial conditions for central collisions does not change significantly with the progression of time because the initial system is symmetric. However, the nature of the power spectrum for MCG initial condition with negligible values for odd l 's changes substantially showing similar magnitudes for odd and even l 's. The power spectrum for perturbation introduced through phase space distribution which take the system away from equilibrium has also been estimated. It has been observed that the temperature variation of power spectrum with perturbation is distinctly different from the one without perturbation - clearly indicating the trace of non-equilibration in the system. Such studies will help in constraining the initial states [62, 63]. A relation between the power spectrum with the flow harmonics has been derived. This relation can be used to estimate the pseudo-rapidity and p_T dependence of the flow harmonics. The power spectrum of phase space perturbation can be used to estimate the fluctuations in flow harmonics and its dependence on kinematic variables.

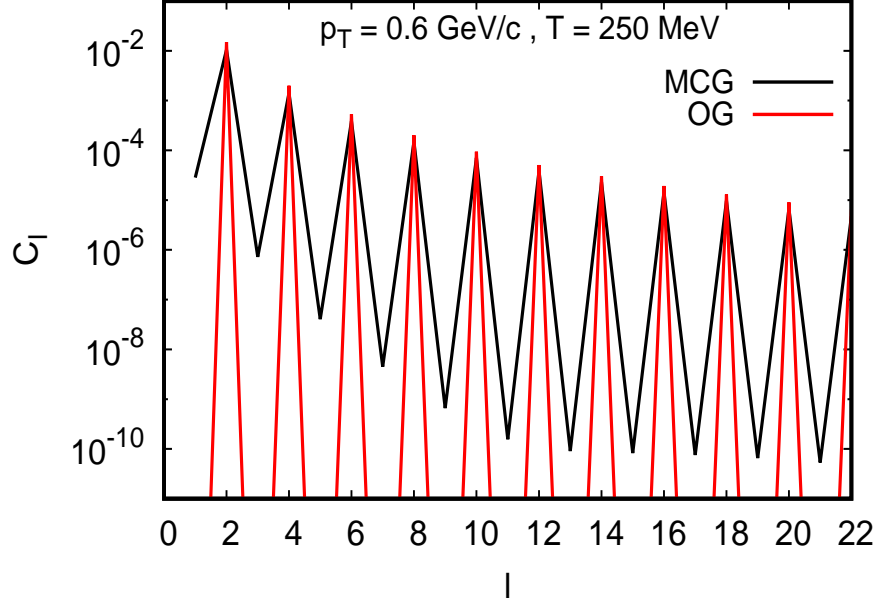


FIG. 11: Same as Fig. 10 at $T = 250$ MeV.

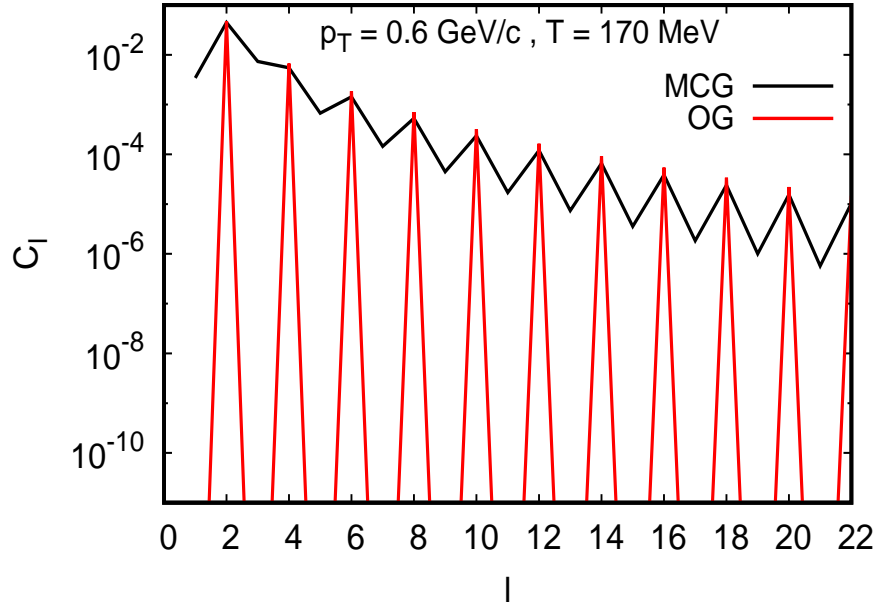


FIG. 12: Same as Fig. 10 at $T = 170$ MeV.

VII. APPENDIX A

In this appendix we provide the expressions for f_n 's appearing in Eq. 8.

$$f_0 = 1 + \frac{3N_f}{32}(7 + 120\hat{\mu}_q^2 + 240\hat{\mu}_q^4) \quad (32)$$

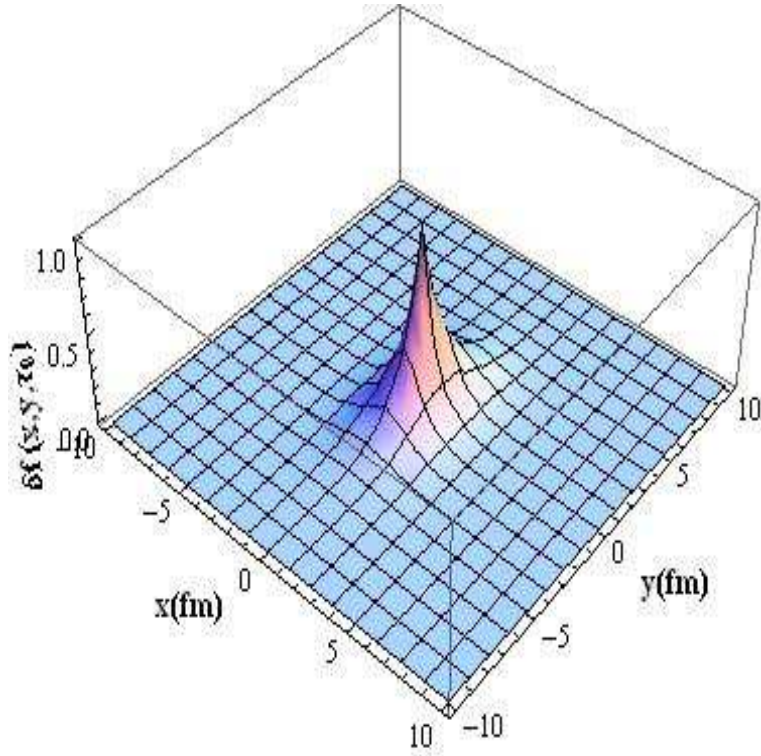


FIG. 13: The initial perturbation δf given in Eq. 22 with $n = 2$.

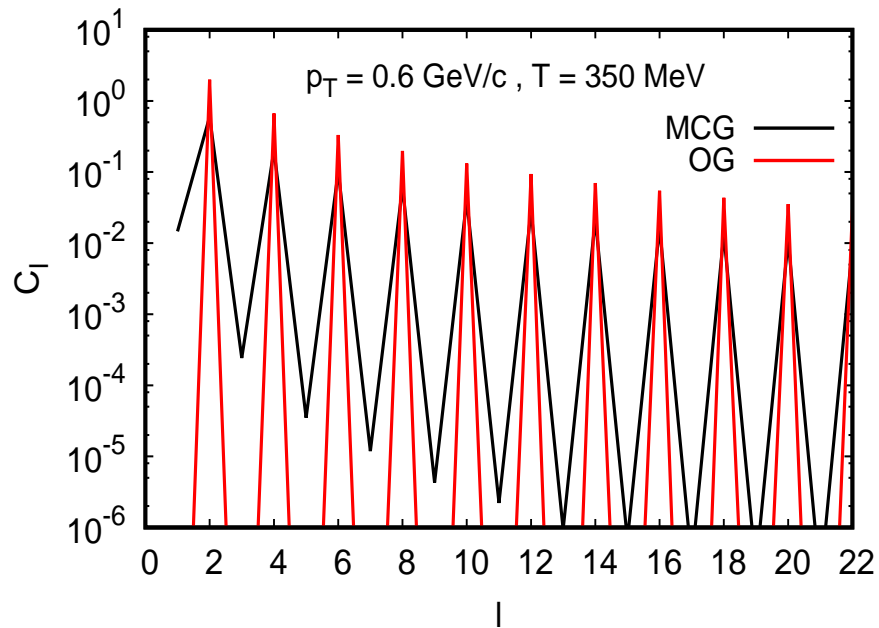
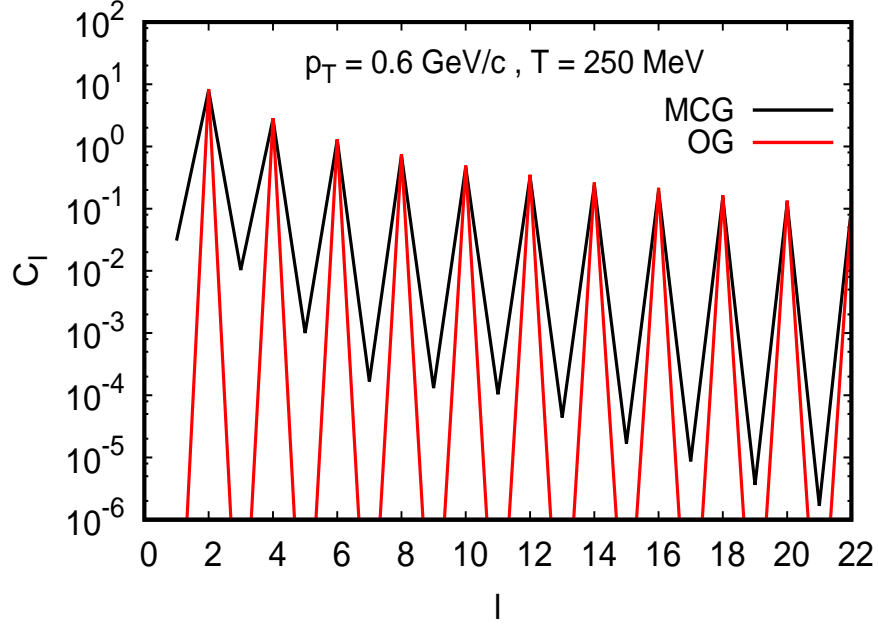
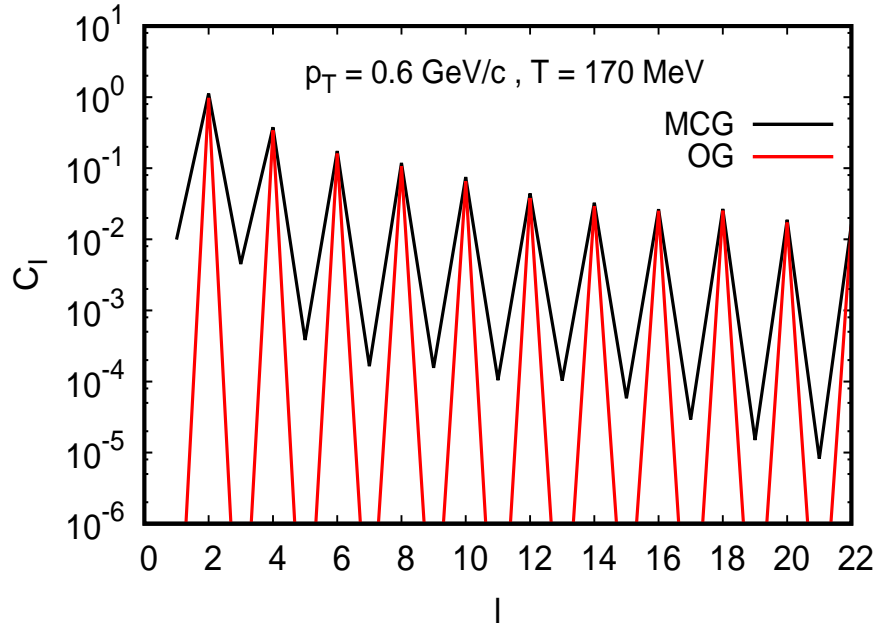
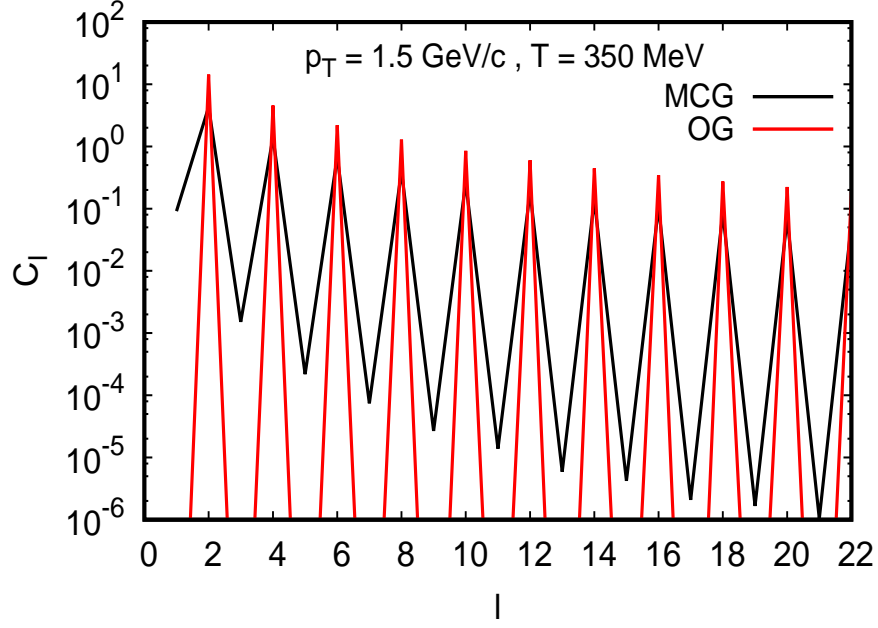
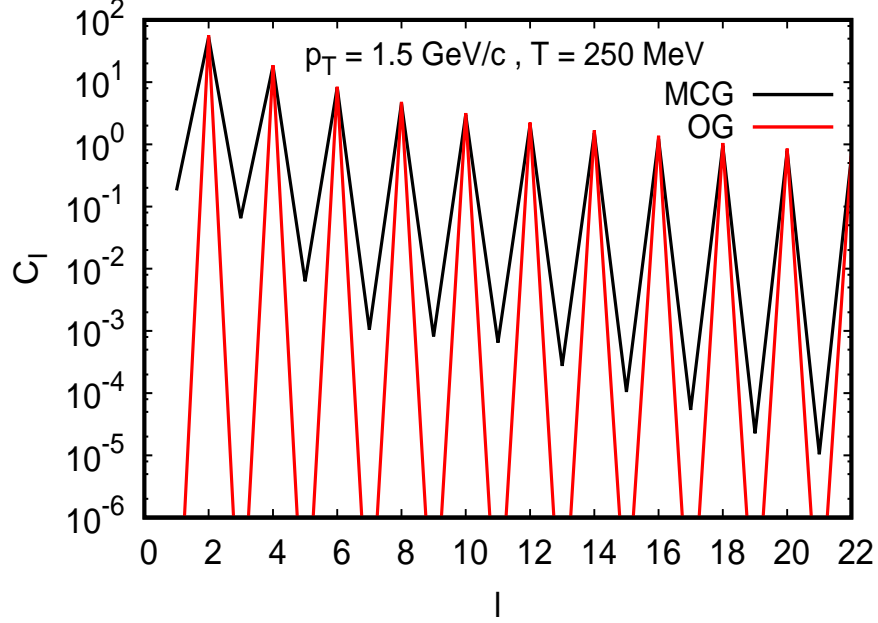


FIG. 14: The power spectrum of the perturbation at $T = 350$ MeV for perturbation shown in Fig 12. The red (black) line shows results for OG (MCG) initial conditions for $p_T = 0.6$ GeV/ c

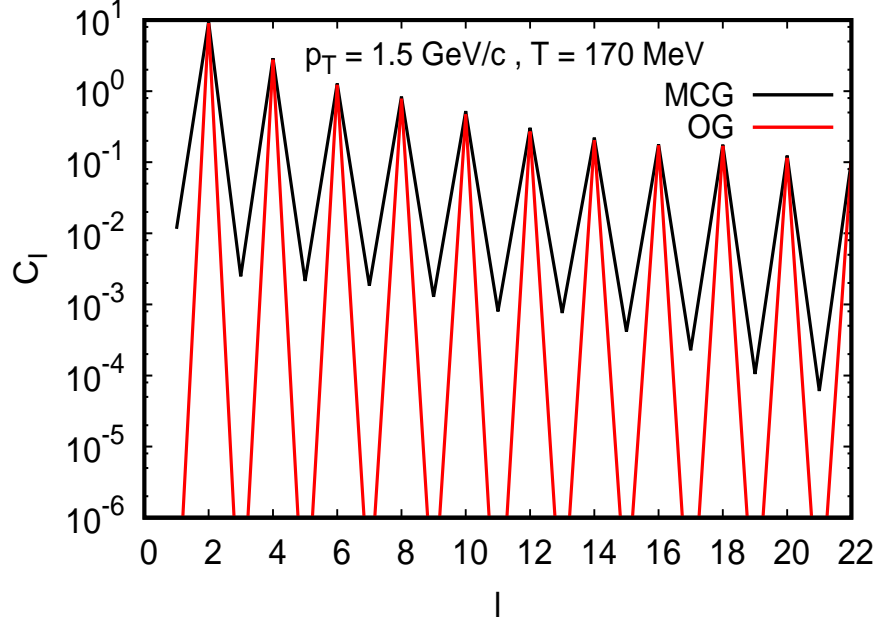
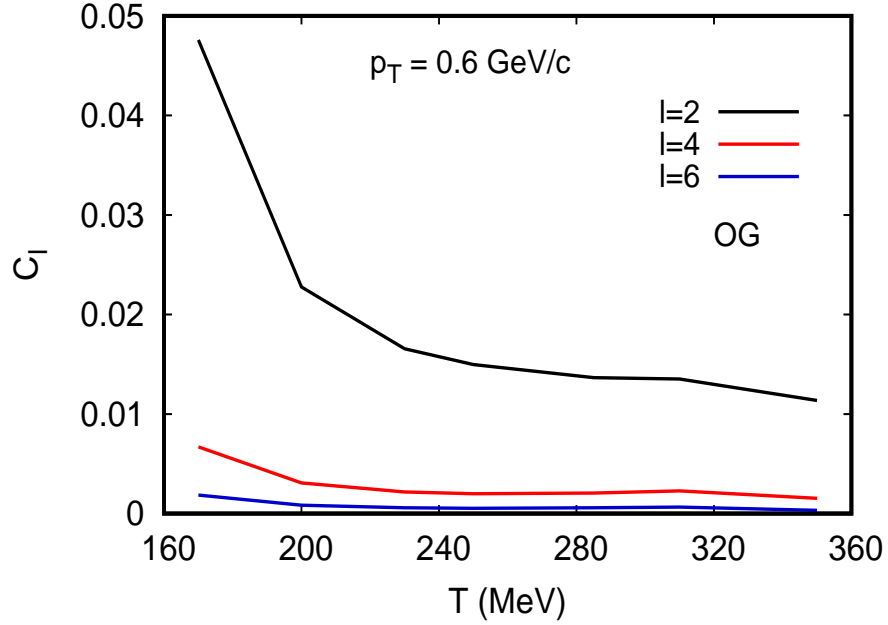
FIG. 15: Same as Fig 14 at $T = 250$ MeVFIG. 16: Same as Fig. 10 at $T = 170$ MeV.

$$f_2 = -\frac{15}{4} \left[1 + \frac{N_f}{12} (5 + 72\hat{\mu}_q^2 + 144\hat{\mu}_q^4) \right] \quad (33)$$

$$f_3 = 30 \left[1 + \frac{N_f}{6} (1 + 12\hat{\mu}_q^2) \right]^{3/2} \quad (34)$$

FIG. 17: Same as Fig 14 for $p_T = 1.5 \text{ GeV}/c$ FIG. 18: Same as Fig 15 at $T = 170 \text{ MeV}$

$$\begin{aligned}
f_4 = & 237.223 + (15.963 + 124.773\hat{\mu}_q^2 - 319.849\hat{\mu}_q^4)N_f - (0.415 + 15.926\hat{\mu}_q^2 + 106.719\hat{\mu}_q^4)N_f^2 \\
& + \frac{135}{2} \left[1 + \frac{N_f}{6}(1 + 12\hat{\mu}_q^2) \right] \ln \left[\left(\frac{\alpha_s}{\pi} \right) \left(1 + \frac{N_f}{6}(1 + 12\hat{\mu}_q^2) \right) \right] \\
& - \frac{165}{2} \left[1 + \frac{N_f}{12}(5 + 72\hat{\mu}_q^2 + 144\hat{\mu}_q^4) \right] \left(1 - \frac{2N_f}{33} \right) \ln \hat{M}
\end{aligned} \tag{35}$$

FIG. 19: Same as Fig 16 for $p_T = 1.5 \text{ GeV}/c$ FIG. 20: The temperature variation of power spectrum with OG initial condition for different l values.

$$\begin{aligned}
 f_5 = & -\sqrt{1 + \frac{N_f}{6}(1 + 12\hat{\mu}_q^2)[799.149 + (21.963 - 137.33\hat{\mu}_q^2 + 482.171\hat{\mu}_q^4)N_f]} \\
 & + (1.926 + 2.0749\hat{\mu}_q^2 - 172.07\hat{\mu}_q^4)N_f^2 + \frac{495}{12}[6 + N_f(1 + 12\hat{\mu}_q^2)] \left(1 - \frac{2N_f}{33}\right) \ln \hat{M}
 \end{aligned} \tag{36}$$

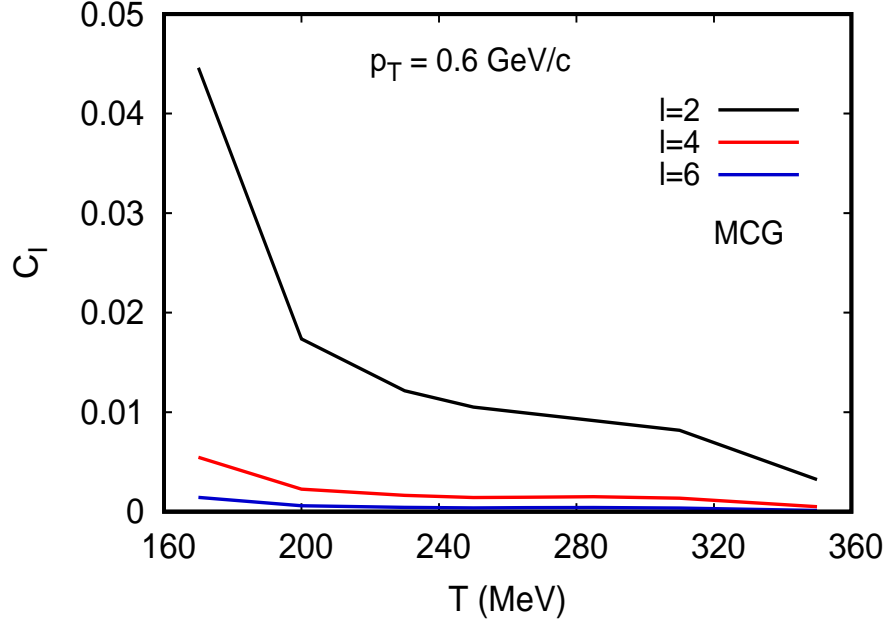


FIG. 21: The variation of power spectrum for even l with temperature for MCG initial condition.

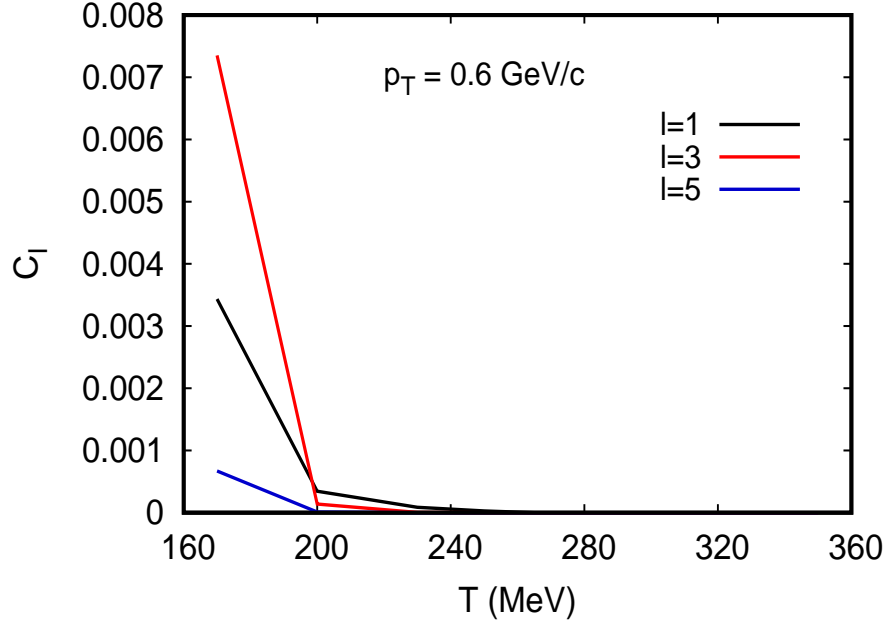


FIG. 22: The variation of power spectrum for odd l with temperature for MCG initial condition.

$$\begin{aligned}
 f_6 = & - \left[659.175 + (65.888 - 341.489\hat{\mu}_q^2 + 1446.514\hat{\mu}_q^4)N_f + (7.653 + 16.225\hat{\mu}_q^2 - 516.210\hat{\mu}_q^4)N_f^2 \right. \\
 & - \frac{1485}{2} \left(1 + \frac{N_f}{6}(1 + 12\hat{\mu}_q^2) \right) \left(1 - \frac{2N_f}{33} \right) \ln \hat{M} \left. \ln \left[\left(\frac{\alpha_s}{\pi} \right) \left(1 + \frac{N_f}{6}(1 + 12\hat{\mu}_q^2) \right) 4\pi^2 \right] \right. \\
 & \left. - 475.587 \ln \left[\left(\frac{\alpha_s}{\pi} \right) 4\pi^2 C_A \right] \right]
 \end{aligned} \tag{37}$$

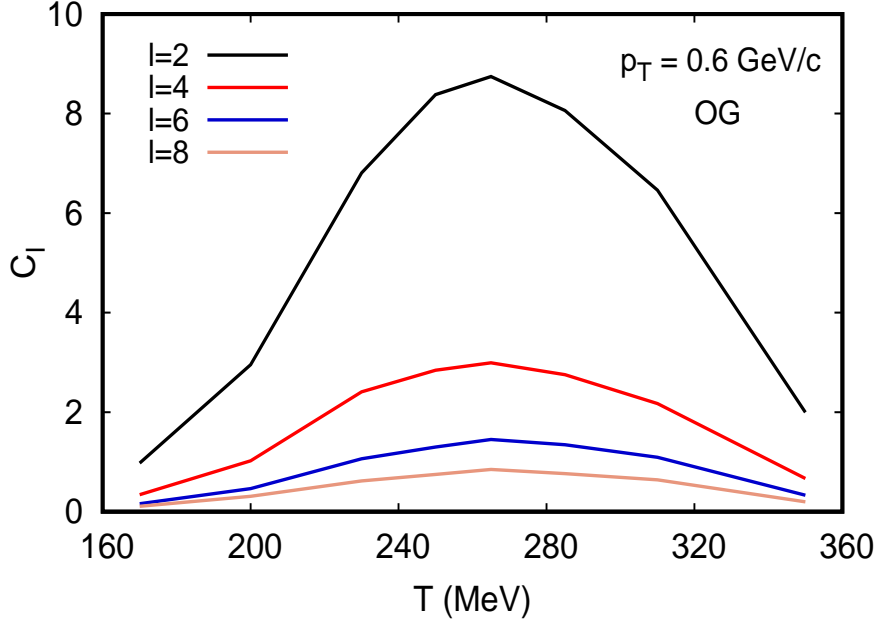


FIG. 23: The variation of power spectrum with temperature for OG initial condition with perturbation at $p_T = 0.6 \text{ GeV}/c$ (see text for details).

VIII. APPENDIX B

In this appendix we derive a relation between anisotropic flow coefficients, v_n and the coefficients, a_{lm} . The transverse momentum (p_T) distribution can be written as:

$$\frac{dN}{d^2p_T dy}(p_T, \theta, \phi) = \frac{1}{2\pi} \frac{dN}{p_T dp_T dy} \left(1 + \sum_{n=1}^{\infty} v_n \cos(n\phi) \right) \quad (38)$$

Moreover, the same quantity can be written as:

$$\frac{dN}{d^2p_T dy}(p_T, \theta, \phi) = \bar{N} + \sum_{l=1}^{\infty} \sum_{m=-l}^l a_{lm} Y_{lm}(\theta, \phi) \quad (39)$$

This gives

$$\frac{1}{2\pi} \frac{dN}{p_T dp_T dy} \left(1 + \sum_{n=1}^{\infty} v_n \cos(n\phi) \right) = \bar{N} + \sum_{l=1}^{\infty} \sum_{m=-l}^l a_{lm} Y_{lm}(\theta, \phi)$$

Multiply either sides by $\cos(k\phi)$ and integrate over ϕ

$$\int_0^{2\pi} d\phi \cos(k\phi) \frac{1}{2\pi} \frac{dN}{p_T dp_T dy} \left(1 + \sum_{n=1}^{\infty} v_n \cos(n\phi) \right) = \int_0^{2\pi} d\phi \cos(k\phi) \left(\bar{N} + \sum_{l=1}^{\infty} \sum_{m=-l}^l a_{lm} Y_{lm}(\theta, \phi) \right)$$

This gives

$$\frac{1}{2\pi} \frac{dN}{p_T dp_T dy} \int_0^{2\pi} d\phi \cos(k\phi) \sum_{n=1}^{\infty} v_n \cos(n\phi) = \int_0^{2\pi} d\phi \cos(k\phi) \sum_{l=1}^{\infty} \sum_{m=-l}^l a_{lm} Y_{lm}(\theta, \phi)$$

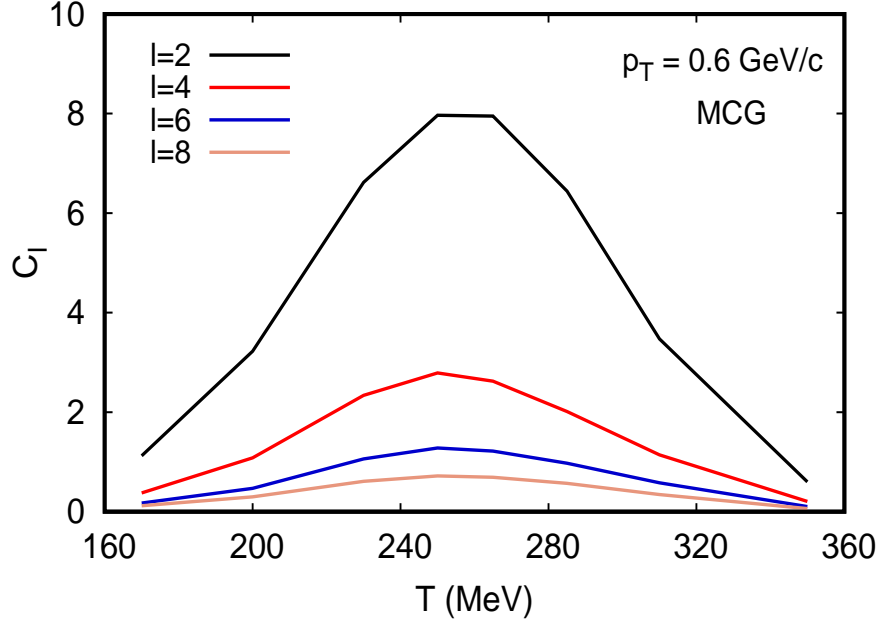


FIG. 24: The variation of power spectrum of even l with temperature for MCG initial condition with perturbation at $p_T = 0.6$ GeV/ c (see text for details).

$$\frac{1}{2\pi} \frac{dN}{p_T dp_T dy} v_k = \int_0^{2\pi} d\phi \cos(k\phi) \sum_{l=1}^{\infty} \sum_{m=-l}^l a_{lm} Y_{lm}(\theta, \phi)$$

$$\frac{1}{2\pi} \frac{dN}{p_T dp_T dy} v_k = \int_0^{2\pi} d\phi \cos(k\phi) \sum_{l=1}^{\infty} \sum_{m=-l}^l a_{lm} \sqrt{\frac{2l+1}{4\pi} \frac{(l-m)!}{(l+m)!}} P_l^m(\cos \theta) [\cos(m\phi) + i \sin(m\phi)]$$

$$\frac{1}{2\pi} \frac{dN}{p_T dp_T dy} v_k = \sum_{l \geq k}^{\infty} \sqrt{\frac{2l+1}{4\pi}} \left[a_{l,k} \sqrt{\frac{(l-k)!}{(l+k)!}} P_l^k(\cos \theta) + a_{l,-k} \sqrt{\frac{(l+k)!}{(l-k)!}} P_l^{-k}(\cos \theta) \right]$$

$$\frac{1}{2\pi} \frac{dN}{p_T dp_T dy} v_k = \sum_{l \geq k}^{\infty} \sqrt{\frac{2l+1}{4\pi} \frac{(l-k)!}{(l+k)!}} [a_{l,k} + (-1)^k a_{l,-k}] P_l^k(\cos \theta)$$

-
- [1] J. C. Collins and M. J. Perry, Phys. Rev. Lett. **34**, 1353 (1975).
[2] D. J. Gross and F. Wilczek, Phys. Rev. Lett. **30**, 1343 (1973).
[3] H. D. Politzer, Phys. Rev. Lett. **30**, 1346 (1973).
[4] A. Bazavov et al., Phys. Rev. D **90**, 094503 (2014).
[5] S. Borsanyi, Z. Fodor, C. Hoelbling, S. D. Katz, S. Krieg and K. K. Szabo, Phys. Lett. B **730**, 99 (2014).
[6] F. Karsch and E. Laermann, hep-lat/0305025.
[7] W. Hu and S. Dodelson, Ann. Rev. Astron. Astrophys. **40**, 171 (2002).
[8] R. Durrer, The Cosmic Microwave Background, Cambridge University Press, 2008.
[9] C. -P. Ma and E. Bertschinger, Astro. Phys. J. **455**, 7 (1995).
[10] A. P. Mishra, R. K. Mohapatra, P. S. Saumia and A. M. Srivastava, Phys. Rev. C **77**, 064902 (2008).
[11] A. Mocsy and P. Sorensen, Nucl. Phys. A **855**, 241 (2011).
[12] P. Naselsky et al., Phys. Rev. C **86**, 024916 (2012).

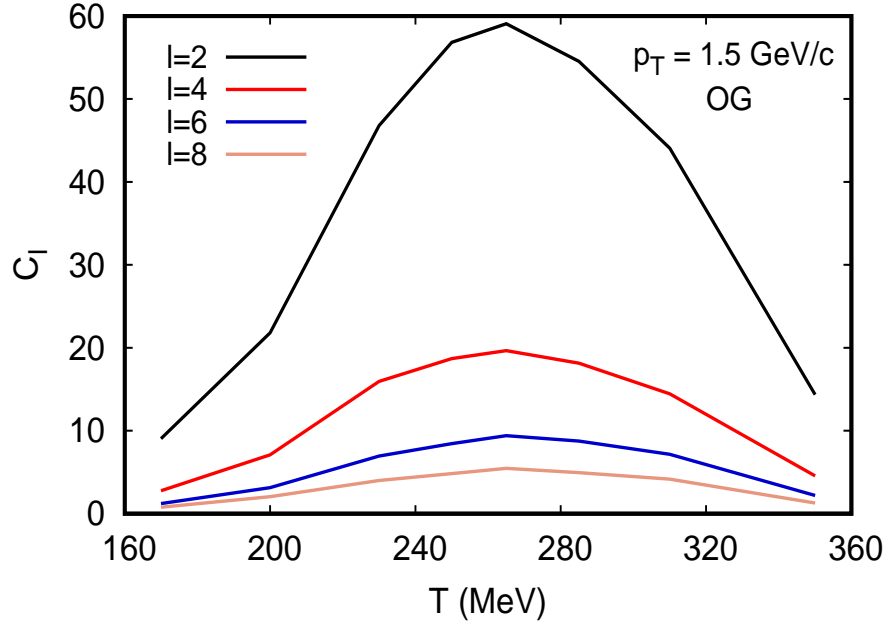


FIG. 25: Same as Fig 23 for $p_T = 1.5$ GeV/c

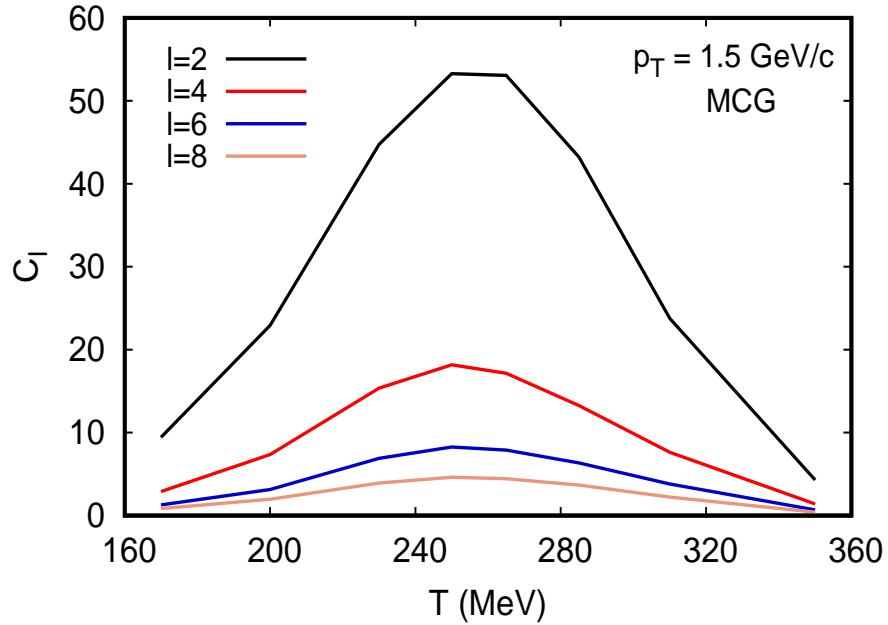


FIG. 26: Same as Fig 24 for $p_T = 1.5$ GeV/c

- [13] F. J. Llanes-Estrada and J. L. M. Martinez, rXiv:1612.05036 [hep-ph].
- [14] X.-N. Wang and M. Gyulassy, Phys. Rev. D **44**, 3501 (1991).
- [15] M. A. Stephanov, K. Rajagopal and E. V. Shuryak, Phys. Rev. Lett. **81**, 4816 (1998).
- [16] M. A. Stephanov, K. Rajagopal and E. V. Shuryak, Phys. Rev. D **60**, 114028 (1999).
- [17] M. A. Stephanov, Phys. Rev. D **81**, 054012 (2010).
- [18] M. Asakawa, U. Heinz and B. Muller, Phys. Rev. Lett. **85**, 2072 (2000).
- [19] S. Jeon and V. Koch, Phys. Rev. Lett. **83**, 5435 (1999).

- [20] S. Jeon and V. Koch, Phys. Rev. Lett. **85**, 2076 (2000).
- [21] S. Mrowczynski, Phys. Rev. C **57**, 1518 (1998).
- [22] G.-Y. Qin and B. Mueller, Phys. Rev. C **85**, 061901(R) (2012).
- [23] P. Staig and E. Shuryak, Phys. Rev. C **84**, 034908; Phys. Rev. C **84**, 044912 (2011).
- [24] A. Rafiei and K. Javidan, Phys. Rev. C **94**, 034904 (2016).
- [25] J. I. Kapusta, B. Muller and M. Stephanov, Phys. Rev. C **85**, 054906 (2012).
- [26] S. Shi, J. Liao and P. Zhuang, Phys. Rev. C **90**, 064912 (2014).
- [27] S. Floerchinger and U. A. Wiedemann, Phys. Rev. C **88**, 044906 (2013); S. Floerchinger and U. A. Wiedemann, Phys. Lett. B **728**, 407 (2014).
- [28] S. Shi, J. Liao, and P. Zhuang, Phys. Rev. C **94**, 034904 (2016).
- [29] M. Luzum and H. Petersen J. Phys. G: Nucl. Part. Phys. **41** (2014) 063102 (41pp)
- [30] M. L. Miller, K. Reygers, S. J. Sanders and P. Steinberg, Ann. Rev. Nucl. Part. Sci. **57**, 205 (2007). DOI:10.1146/annurev.nucl.57.090506.123020
- [31] M. Bleicher *et al.*, J. Phys. G. **25**, 1859 (1999).
- [32] J. Adams *et al.*, Phys. Rev. Lett., **97**(16), [162301]
- [33] Iu. Karpenko, P. Huovinen, M. Bleicher, Comp. Phys. Comm. **185**, 3016 (2014).
- [34] J. D. Bjorken, Phys. Rev. D **27**, 140 (1983).
- [35] M. Albright, J. Kapusta and C. Young, Phys. Rev. C **56**, 024915 (2014)
- [36] G. D. Yen, M. I. Gorenstein, W. Greiner and S.N. Yang, Phys. Rev. C **56** (1997) 2210
- [37] A. Vuorinen, Phys. Rev. D **67**, 074032 (2003); **68**, 054017 (2003)
- [38] N. Haque, M. G. Mustafa and M. Strickland, Phys. Rev. D **87**, 105007 (2013)
- [39] Y. Hama, T. Kodama and O. Socolowski Jr., Brazilian Journal of Physics, vol. 35, no. 1 (2005)
- [40] Particle data Group, J. Beringer *et al.*, Phys. Rev. D. **86**, 010001 (2012).
- [41] S. Borsányi *et al.*, Phys. Lett. B **370** (2014) 99-104
- [42] E. M. Lifshitz and L. P. Pitaevskii, Physical Kinetics (Elsevier, New York, 1987).
- [43] S. R. de Groot, W. A. van Leeuwen and C. G. van Weert, Relativistic kinetic theory : principles and applications, North-Holland Publishing Co., Amsterdam, 1980.
- [44] C. Cercignani and G. M. Kremer, The relativistic Boltzmann equation: theory and applications, Springer Basel AG, 2002.
- [45] G. Sarwar and J. Alam (to be published).
- [46] W. Florkowski, R. Ryblewski, M. Strickland, Phys. Rev. C **88**, 024903 (2013).
- [47] W. Florkowski, R. Ryblewski, M. Strickland, Phys. Rev. D **86**, 085023 (2012).
- [48] Y. Hatta, M. Martinez and B. -W. Xiao, Phys. Rev. D **91**. 085024 (2015).
- [49] G.S. Denicol *et al.*, Phys. Rev. Lett. **113**, 202301 (2014)
- [50] D. Bazow *et al.*, Phys. Rev. Lett. **116**, 022301 (2016)
- [51] J. Tindall, J. M. Torres-Rincon, J. B. Rose and H. Petersen, Phys. Lett. B **770**, 532 (2017).
- [52] H. Levine, Partial Differential Equations, American Mathematical Society (1997).
- [53] M. H. Thoma, Phys. Rev. D **49**, 451 (1994).
- [54] F. Cooper, G. Frye, Phys. Rev. D **10** (1974) 186.
- [55] S. Jeon and U. Heinz, Int. J. Mod. Phys. E **24**, 1530010 (2015),
- [56] J. Adam *et al.* (for ALICE collaboration) Phys. Rev. Lett. **117**, 182301 (2016).
- [57] N. Borghini, J.Y. Ollitrault, Phys. Lett. B **642**, 227 (2006).
- [58] U. Heinz and R. Snellings, Ann. Rev. Nucl. Part. Sci. **63**, 63 (2013).
- [59] P. B. Arnold, C. Dogan, and G. D. Moore, Phys. Rev. D **74**, 085021 (2006).
- [60] F. G. Gardin, F. Grassi, M. Luzum and J. Noronha-Hostler, Phys. Rev. C **95**, 034901 (2017).
- [61] J. Adams *et al.* (for ALICE collaboration), Phys. Rev. Lett. **117** 182310 (2016).
- [62] E. Retinsaya, M. Luzum and J. Y. Ollitrault, Phys. Rev. C **89**, 014902 (2014).
- [63] H. Petersen, C. Coleman-Smith, S. A. Bass and R. Wolpert, J. Phys. G **58**, 045102 (2011).